Silicon (2023) 15:5891–5909
https://doi.org/10.1007/s12633-023-02487-3

RESEARCH

Efficient Removal and Preconcentration of Pd(II) Ions in Environmental Water Using Co_2SiO_4 Nanoparticles Modified by Mordant Red 3 as a Novel Adsorbent

Faisal K. Algethami[1]

Received: 9 February 2023 / Accepted: 20 April 2023 / Published online: 29 April 2023

Abstract
In this work, Co_2SiO_4 nanoparticles were facilely synthesized using the pechini sol gel method then modified by mordant red 3 as a novel composite for the separation and efficient preconcentration of palladium(II) ions from the aqueous chemical solutions prior to their determination by atomic absorption spectrometry. The synthesized products were characterized by X-ray diffraction (XRD), Fourier-transform infrared spectroscopy (FT-IR), transmission electron microscope (TEM), scanning electron microscope (SEM), and CHN elemental analysis. The successful modification of the Co_2SiO_4 nanoparticles by mordant red 3 was demonstrated by the appearance of a wide XRD peak centered at $2\Theta=24^{o}$, SEM morphological change to flower-like shapes, the presence of carbon (C) and nitrogen (N), and the presence of characteristic organic functional groups using FT-IR. The maximum elimination capability of the synthesized nanocomposite towards palladium (II) ions is 166.39 mg/g. The adsorption of palladium (II) ions is spontaneous, chemical, and can be adequately described using the pseudo-second order kinetic model and Langmuir equilibrium isotherm. The nanocomposite was regenerated at least five times with a 0.5 M thiourea solution without a notable decrease in the % removal. The results confirmed that the optimized procedure is accurate (% recovery > 95%), reproducible (% RSD < 3.5%), and has a 0.5–450 µg/L dynamic linear range.

Keywords Co_2SiO_4 nanoparticles · Mordant red 3 · Preconcentration · Pd(II) ions · Adsorption

1 Introduction

Palladium metal is recognized as an important element that has distinctive features. It is combined with some metals to produce dental alloys, jewelry, and catalytic car converters [1, 2]. Depending on the method of the contact and chemical type of palladium, exposure to palladium or its derivatives may cause harmful effects on the eyes, skin, kidneys, lungs, bone marrow, and liver [3]. There are numerous techniques for measuring palladium, including flame atomic absorption spectrometry, spectrophotometry, inductively coupled plasma-optical emission spectrometry, and inductively coupled plasma-mass spectrometry [4–7]. Owing to the existence of a complex matrix including the analyte and low sensitivity, the majority of these procedures are inappropriate for the direct determination of palladium in real environmental samples. Preconcentration of palladium prior to analysis is a crucial step for enhancing selectivity and sensitivity. Various approaches depending on chemical, physical, or physicochemical concepts, such as cloud point extraction, high-performance liquid chromatography, solid phase extraction, and liquid-liquid extraction, were utilized to accomplish this goal [8–11]. The need to get contaminants out of water sources so that potable water can be made has led to the development of several ways to clean water. The solid phase extraction method has gotten a lot of attention due to its simplicity, low cost, and effectiveness [12, 13]. There are many adsorbents that are used to separate palladium ions such as cross-linked chitosan into graphene oxide-iron(III) oxide hydroxide, ion-imprinted modified chitosan resin, grafted cellulose with glycidyl methacrylate and N-isopropylacrylamide, and phosphine-functionalized Fe_3O_4/SiO_2composite [14–17]. Recently, the modification of solid supports, such as SiO_2 and zeolite nanoparticles, by organic compounds to improve their adsorption capacities toward several metal ions has gained

✉ Faisal K. Algethami
falgethami@imamu.edu.sa

[1] Department of Chemistry, College of Science, Imam Mohammad Ibn Saud Islamic University (IMSIU), Riyadh 11623, Saudi Arabia

considerable study attention [12, 13, 18, 19]. Co_2SiO_4 nanoparticles is used in many fields, such as ceramics, electrical conduction, lithium batteries, enhanced oxygen evolution, and degradation of organic dyes, for its ability to withstand high temperatures [20–23]. It possesses an orthorhombic shape, consisting of a hexagonal closed-packed oxygen array in which cobalt atoms occupy half of the octahedral positions [24]. The pechini sol gel chemical method is extensively used to prepare various nanomaterials such as Al_2O_3, SiO_2, Fe_2O_3, $Bi_2ZnB_2O_7$, $CoFe_2O_4/SiO_2/Dy_2Ce_2O_7$, ZrO_2/Al_2O_3, and CeO_2/Al_2O_3 [25–29]. In this method, chelates are formed between metal ions and hydroxycarboxylic acids such as citric acid. Then, acid esterification occurs using polyhydroxyl alcohols such as ethylene glycol to obtain a three-dimensional network. Finally, the solvent was evaporated and calcination was performed to degrade the organic fraction and obtain nanoparticles. The surface of the Co_2SiO_4 nanoparticles contains silanol groups (Si-OH) that have the ability to interact with (3-aminopropyl) trimethoxysilane. Besides, the amino group of (3-aminopropyl) trimethoxysilane enables scientists to load many organic materials. These loaded organic materials can easily separate many metal ions by forming chelates between their active groups (such as OH and C=N) and the target metal ions. Consequently, in this work, Co_2SiO_4 nanoparticles were synthesized using the pechini sol gel method then modified by mordant red 3 as a novel composite for the elimination and preconcentration of palladium (II) ions from several samples prior to their estimation by atomic absorption spectrometry.

2 Experimental

2.1 Chemicals

Tetraethyl orthosilicate ($SiC_8H_{20}O_4$), tartaric acid ($C_4H_6O_6$), cobalt(II) acetate tetrahydrate ($C_4H_6CoO_4.4H_2O$), ethylene glycol ($C_2H_6O_2$), ammonium hydroxide (NH_4OH), (3-aminopropyl)trimethoxysilane ($C_6H_{17}NO_3Si$), mordant red 3 ($C_{14}H_7NaO_7S$), palladium(II) chloride ($PdCl_2$), hydrochloric acid (HCl), toluene (C_7H_8), ethanol (C_2H_6O), thiourea (CH_4N_2S), sodium chloride (NaCl), potassium chloride (KCl), magnesium(II) chloride hexahydrate ($MgCl_2.6H_2O$), nickel(II) chloride hexahydrate ($NiCl_2.6H_2O$), cadmium(II) nitrate tetrahydrate ($Cd(NO_3)_2.4H_2O$), cobalt(II) chloride hexahydrate ($CoCl_2.6H_2O$), lead(II) nitrate ($Pb(NO_3)_2$), barium(II) chloride dihydrate ($BaCl_2.2H_2O$), copper(II) chloride dihydrate ($CuCl_2.2H_2O$), iron(III) nitrate nonahydrate ($Fe(NO_3)_3.9H_2O$), chromium(III) nitrate nonahydrate ($Cr(NO_3)_3.9H_2O$), sodium sulfate (Na_2SO_4), sodium bicarbonate ($NaHCO_3$), sodium bromide(NaBr), potassium thiocyanate (KSCN), sulfuric acid (H_2SO_4), and ethylenediaminetetraacetic acid disodium salt dihydrate ($C_{10}H_{18}N_2Na_2O_{10}$) were purchased from the Sigma-Aldrich Chemical Company and used as received without further purification.

2.2 Synthesis of Co_2SiO_4 Nanoparticles

1.00 g of $C_4H_6CoO_4.4H_2O$, 0.42 g of $SiC_8H_{20}O_4$, and 1.20 g of $C_4H_6O_6$ were stirred for 15 min in 20 mL of ethylene glycol. After that, the pH was modified to 8 using NH_4OH then the solution was magnetically stirred for 48 hrs. In addition, the precipitate was subsequently centrifuged, washed carefully with distilled water, dried in oven at 70°C, and calcined in muffle at 800°C for 5 hrs.

2.3 Modification of Co_2SiO_4 Nanoparticles by Mordant Red 3

3.00 g of Co_2SiO_4 nanoparticles were magnetically stirred for 15 min in 25 mL of benzylene, then 3 mL of (3-aminopropyl) trimethoxysilane was added. After that, the mixture was refluxed at 150°C for 24 hrs. The Co_2SiO_4/(3-aminopropyl) trimethoxysilane composite was subsequently centrifuged, washed with distilled water and ethanol, and dried at 60°C. Furthermore, Co_2SiO_4/(3-aminopropyl) trimethoxysilane

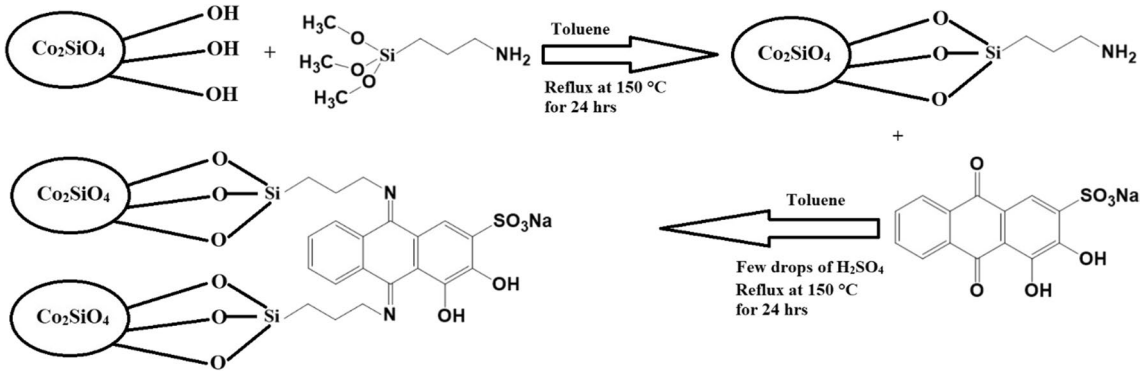

Scheme 1 The utilized chemical steps for the synthesis of the Co_2SiO_4/mordant red 3 nanocomposite

composite and 3 g of mordant red 3 were chemically refluxed at 150°C for 24 hrs in the presence of a little drops of sulfuric acid (H_2SO_4) using 25 mL of benzylene. The Co_2SiO_4/(3-aminopropyl) trimethoxysilane/ mordant red 3 composite was subsequently centrifuged, washed with distilled water and ethanol, and dried at 60°C. Scheme 1 represents the synthetic steps of the Co_2SiO_4/mordant red 3 nanocomposite.

2.4 Adsorption of Palladium (II) Ions

Using a batch technique, the adsorption of palladium (II) ions onto Co_2SiO_4/mordant red 3 nanocomposite was examined. A certain quantity of Co_2SiO_4/mordant red 3 nanocomposite was added to 60 mL of palladium (II) solution. In addition, the mixture was stirred for a period of time before being separated. Using atomic absorption spectrometry, the palladium (II) ion concentration in the supernatant was measured. The % removal of palladium (II) ions was determined using Eq. (1).

$$\% \; removal = \frac{C_o - C_e}{C_o} \times 100 \tag{1}$$

where, C_e (mg/L) and C_o (mg/L) represents the equilibrium and initial concentrations of palladium (II) ions, respectively.

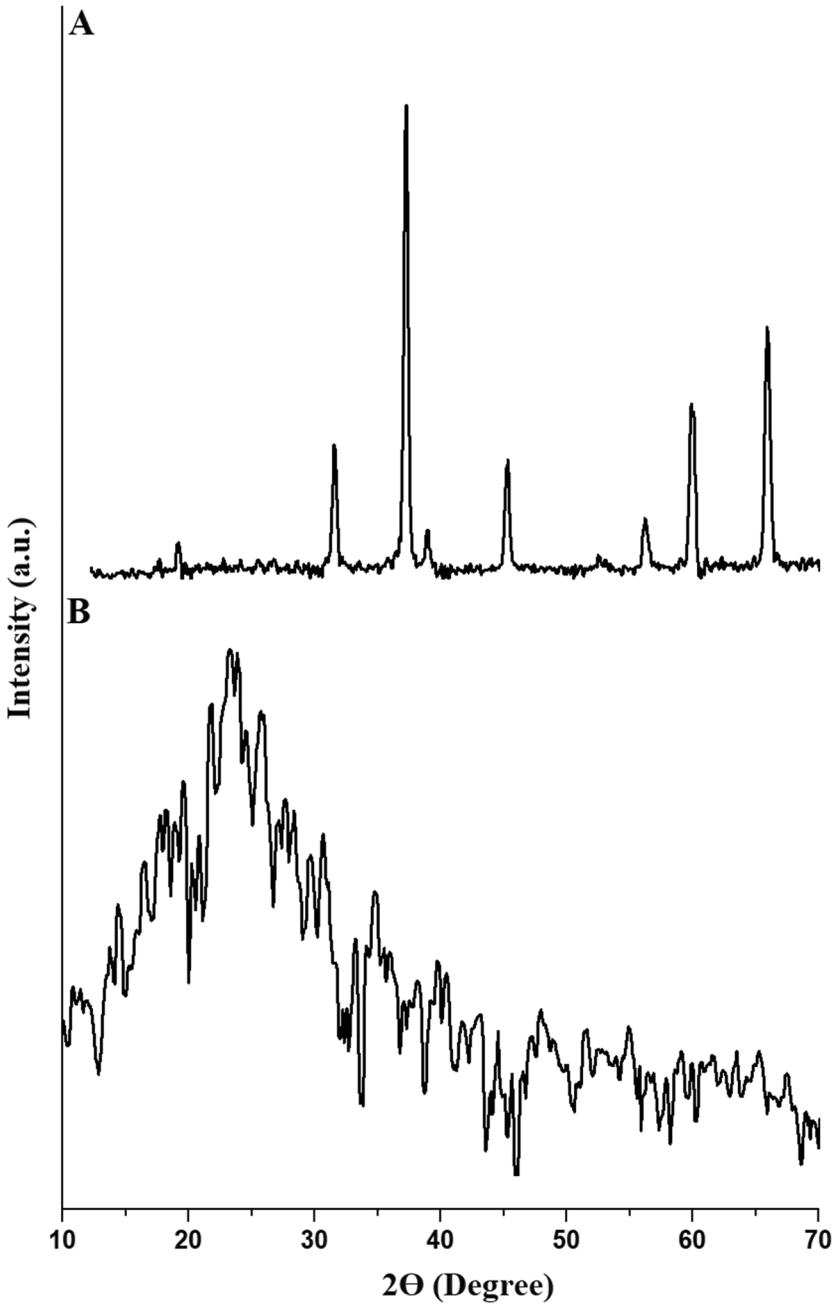

Fig. 1 The obtained XRD peaks of the Co_2SiO_4 nanoparticles (**A**) and Co_2SiO_4/mordant red 3 nanocomposite (**B**)

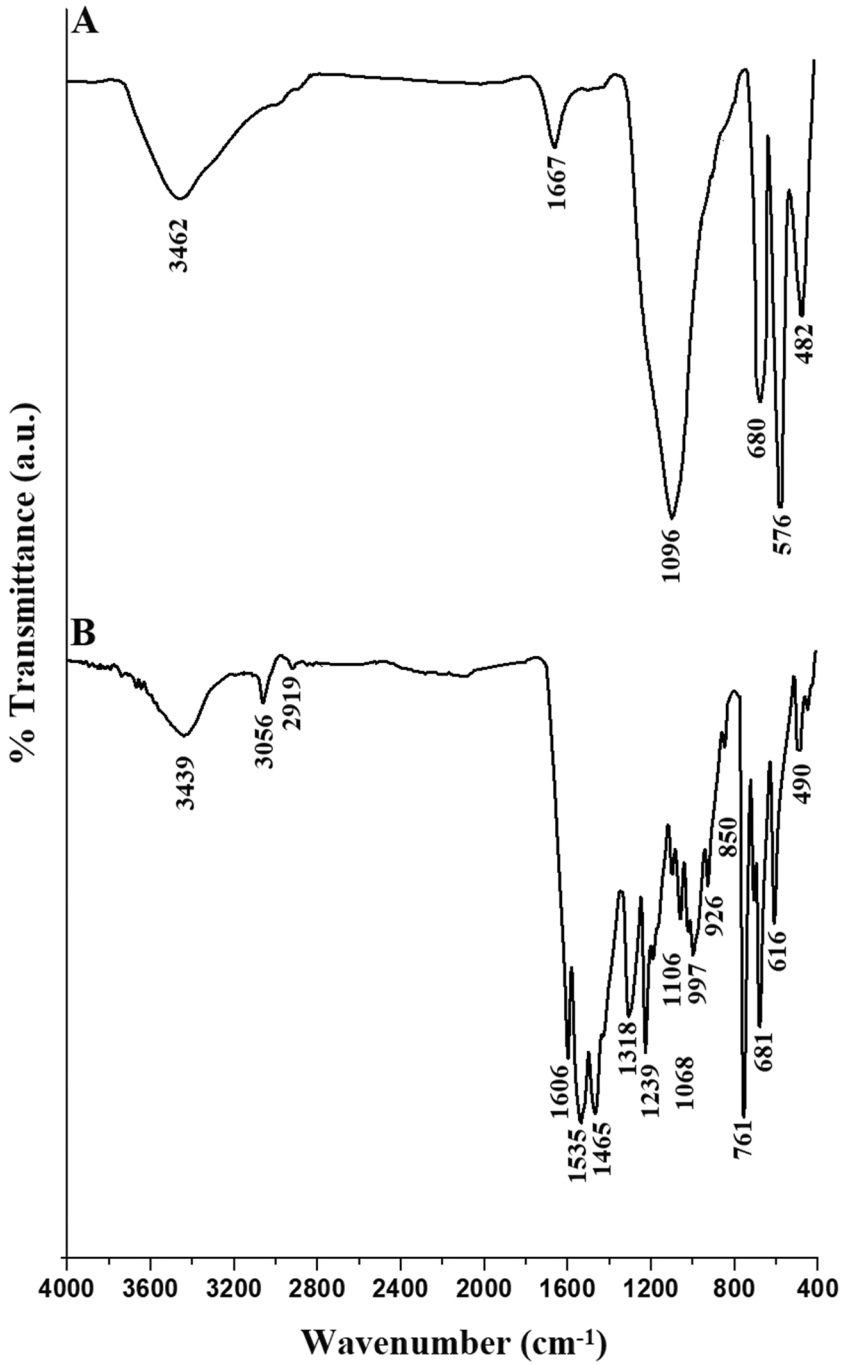

Fig. 2 The obtained FT-IR bands of the Co_2SiO_4 nanoparticles (**A**) and Co_2SiO_4/mordant red 3 nanocomposite (**B**)

From Eq. (2), the elimination capability (Q, mg/g) of the Co_2SiO_4/mordant red 3 nanocomposite was calculated.

$$Q = (C_o - C_e) \times \frac{V}{M} \tag{2}$$

where, V (L) is the volume of palladium (II) solution whereas M(g) is the mass of the Co_2SiO_4/mordant red 3 nanocomposite.

Desorption occurs by stirring the synthesized nanocomposite with 6 mL of specific desorbing agents (Thiourea in addition to ethylenediaminetetraacetic acid disodium salt dihydrate) for 10 min. The desorption efficiency of the Co_2SiO_4/mordant red 3 nanocomposite (% D) was calculated utilizing Eq. (3).

$$\%D = \frac{C_d \times V_d}{(C_o - C_e)V} \times 100 \tag{3}$$

C_d (mg/L) represents the residual concentration of palladium (II) ions in the desorbing agent. V_d (L) represents the utilized volume of the desorbing agent. To

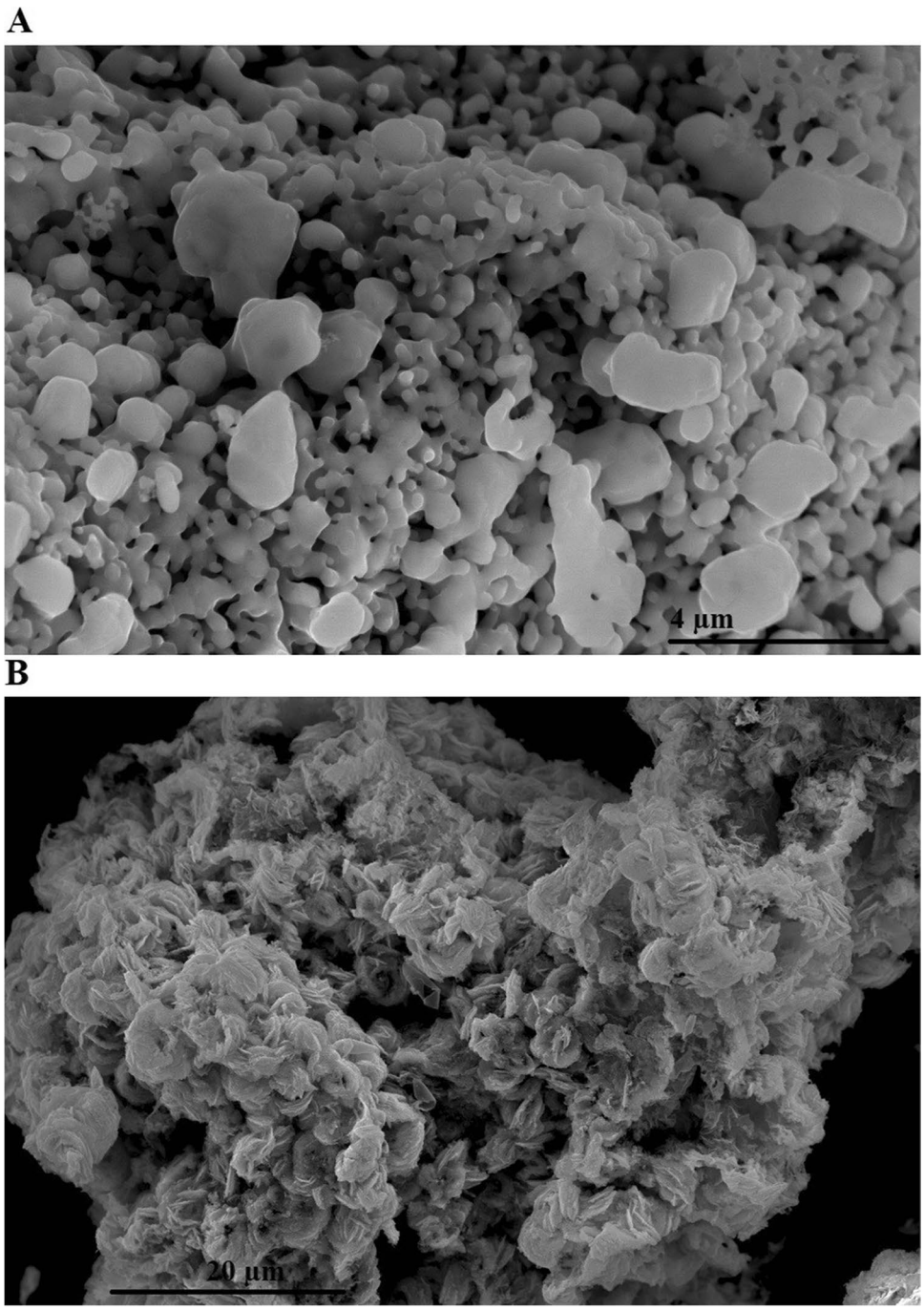

Fig. 3 The obtained SEM pictures of the Co_2SiO_4 nanoparticles (**A**) and Co_2SiO_4/mordant red 3 nanocomposite (**B**)

determine the stability and reusability of the nanocomposite, five cycles of adsorption/desorption were performed. The nanocomposite was rinsed carefully with distilled water after each cycle to prepare it for the subsequent round.

2.5 Instrumentation

The infrared spectra of the Co_2SiO_4 nanoparticles and Co_2SiO_4/mordant red 3 nanocomposite were measured between 4000 and 400 cm^{-1} using KBr discs on an FT-IR spectrometer of model Nicolet. X-ray diffraction (XRD) analyses of the Co_2SiO_4 nanoparticles and Co_2SiO_4/mordant red 3 nanocomposite were conducted exploiting an X-ray diffractometer of model Bruker D_8 Advance. The morphology of the Co_2SiO_4 nanoparticles and Co_2SiO_4/mordant red 3 nanocomposite was investigated using a JSM-IT800 Schottky field scanning electron microscope and a Talos F200iS transmission electron microscope. CHN analysis of the Co_2SiO_4/mordant red 3 nanocomposite was determined using an

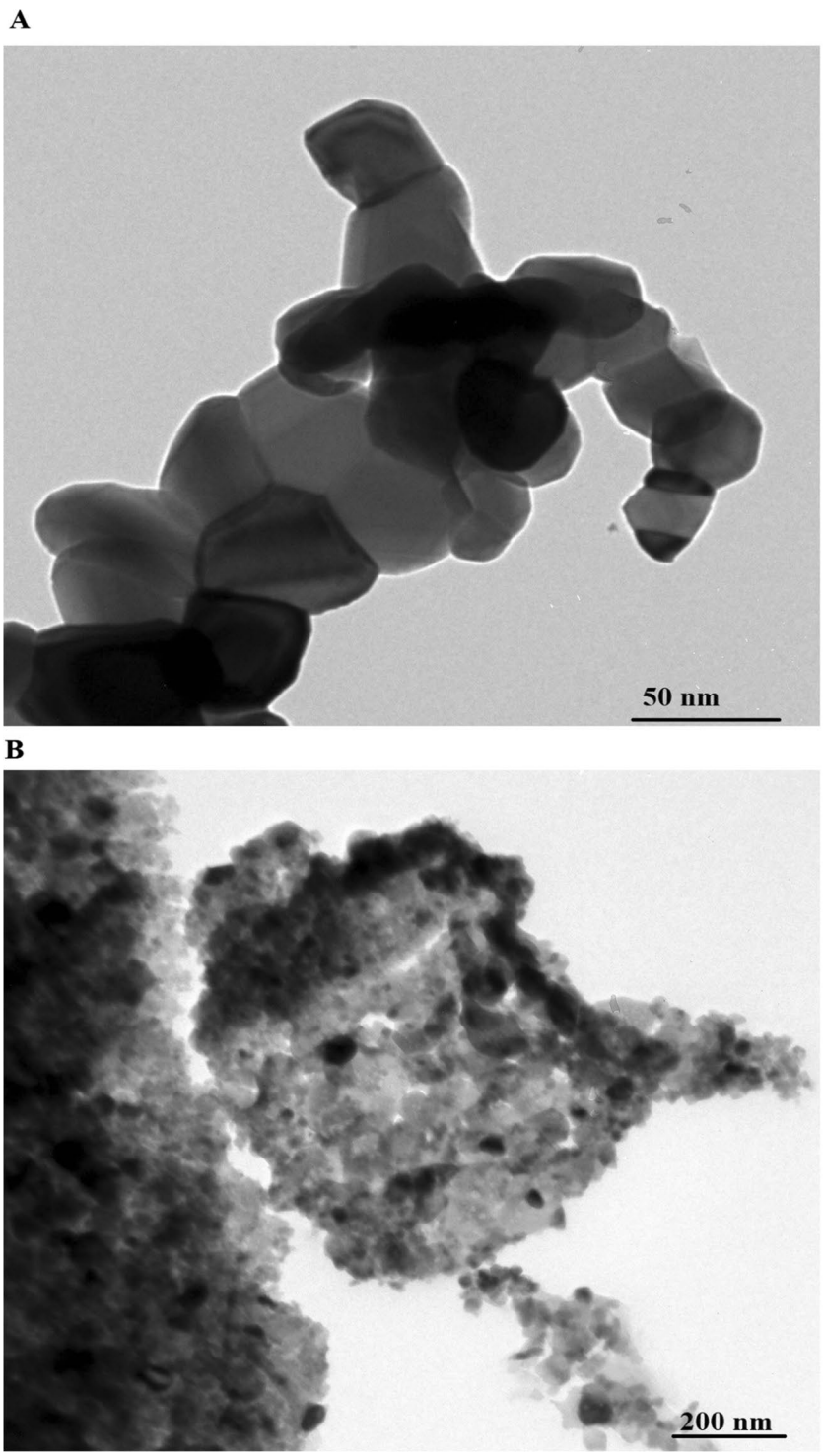

Fig. 4 The obtained TEM pictures of the Co_2SiO_4 nanoparticles (**A**) and Co_2SiO_4/mordant red 3 nanocomposite (**B**)

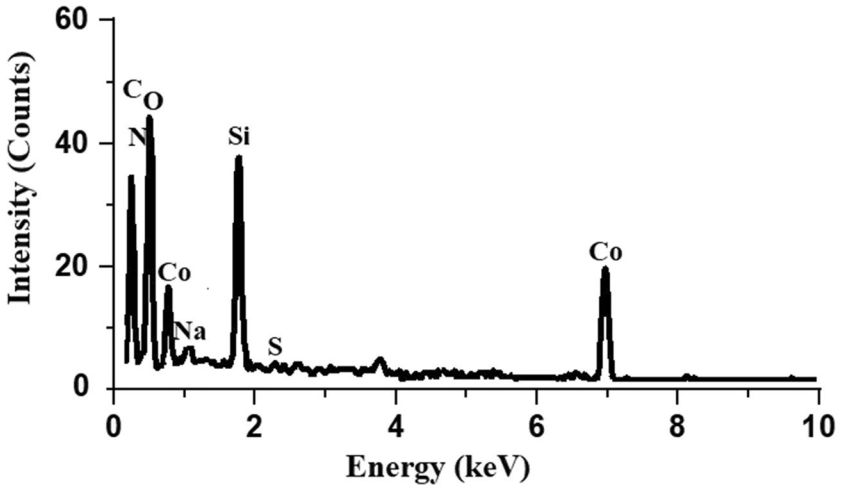

Fig. 5 The EDX analysis of the Co_2SiO_4/mordant red 3 nanocomposite

CHN Elemental Analyzer of model 2400 PerkinElmer. The concentration of palladium (II) solutions was measured at a wavelength of 244.80 nm using an atomic absorption spectrophotometer of model Shimadzu AA-7000F.

3 Results and Discussion

3.1 Characterization of the Fabricated Nanocomposite

Figure 1A-B shows the obtained XRD peaks of the Co_2SiO_4 nanoparticles and Co_2SiO_4/mordant red 3 nanocomposite, respectively. The formed peaks at 2Θ=19.17°, 31.50°, 37.26°, 39.04°, 45.26°, 56.16°, 59.94°, and 65.94° confirm the presence of monoclinic Co_2SiO_4 as clarified from JCPDS No.70-2280. The mean crystal size of the Co_2SiO_4 nanoparticles is 38.27 nm. In addition, the XRD pattern of the Co_2SiO_4/mordant red 3 nanocomposite exhibits a halo at 2Θ=24°. Hence, this confirms that the crystalline chemical structure overlapped or merged with an amorphous ground. Accordingly, this change in XRD patterns proves that the mordant red 3 was successfully loaded onto the Co_2SiO_4 nanoparticles. It is important to note that this observation of the synthesized nanocomposite is the same as many compounds in this family that Ehab and others made [12, 19].

Figure 2A-B shows the obtained FT-IR bands of the Co_2SiO_4 nanoparticles and Co_2SiO_4/mordant red 3 nanocomposite, respectively. In addition, the absorption bands, which were noted in the Co_2SiO_4 nanoparticles, at 482, 576, and 680 cm^{-1} are assigned to the stretching vibration mode of the Co-O. The absorption band, which was observed in the Co_2SiO_4 nanoparticles, at 1096 cm^{-1} is assigned to the stretching vibration mode of the Si-O. The absorption bands, which were observed in the Co_2SiO_4 nanoparticles, at 3462 and 1667 cm^{-1} are assigned to the stretching and bending vibration modes of O-H, respectively. The absorption bands, which were observed in the Co_2SiO_4/mordant red 3 nanocomposite, at 490, 616, and 681 cm^{-1} are assigned to the stretching vibration mode of the Co-O. The absorption bands, which were observed in the Co_2SiO_4/mordant red 3 nanocomposite, at 761, 850, 926, 997, and 1068 cm^{-1} are assigned to the out of plane bending vibration mode of aromatic CH. In addition, the absorption bands, which were observed in the Co_2SiO_4/mordant red 3 nanocomposite, at 1106 and 1239 cm^{-1} are assigned to the stretching vibration modes of the Si-O and S=O, respectively. The absorption band, which was observed in the Co_2SiO_4/mordant red 3 nanocomposite, at 1318 cm^{-1} is assigned to the bending vibration mode of the CH. In addition, the absorption bands, which were noted in the Co_2SiO_4/mordant red 3 nanocomposite, at 1465 and 1535 cm^{-1} are assigned to the stretching vibration mode of aromatic C=C. The absorption band, which was observed in the Co_2SiO_4/mordant red 3 nanocomposite, at 1606 cm^{-1} is assigned to the stretching vibration mode of C=N. The absorption band, which was observed in the Co_2SiO_4/mordant red 3 nanocomposite, at 3439 cm^{-1} is assigned to the stretching vibration mode of OH. Accordingly, this change in FT-IR spectra proves that the mordant red 3 was successfully loaded onto the Co_2SiO_4 nanoparticles [8, 12, 13, 30, 31].

Figure 3A-B shows the obtained SEM pictures of the Co_2SiO_4 nanoparticles and Co_2SiO_4/mordant red 3 nanocomposite, respectively. The results confirm the formation of spheres and irregular shapes with an average grain size of 0.89 µm in the Co_2SiO_4 nanoparticles. Also, the results confirm the formation of a flower-like structure in the Co_2SiO_4/mordant red 3 nanocomposite. Figure 4A-B shows the TEM pictures of the Co_2SiO_4 nanoparticles and Co_2SiO_4/mordant red 3 nanocomposite, respectively. The results confirm the formation of polyhedral and hexagonal shapes with an average diameter of 40.24 nm in the Co_2SiO_4 nanoparticles. Also, the results confirm the formation of a

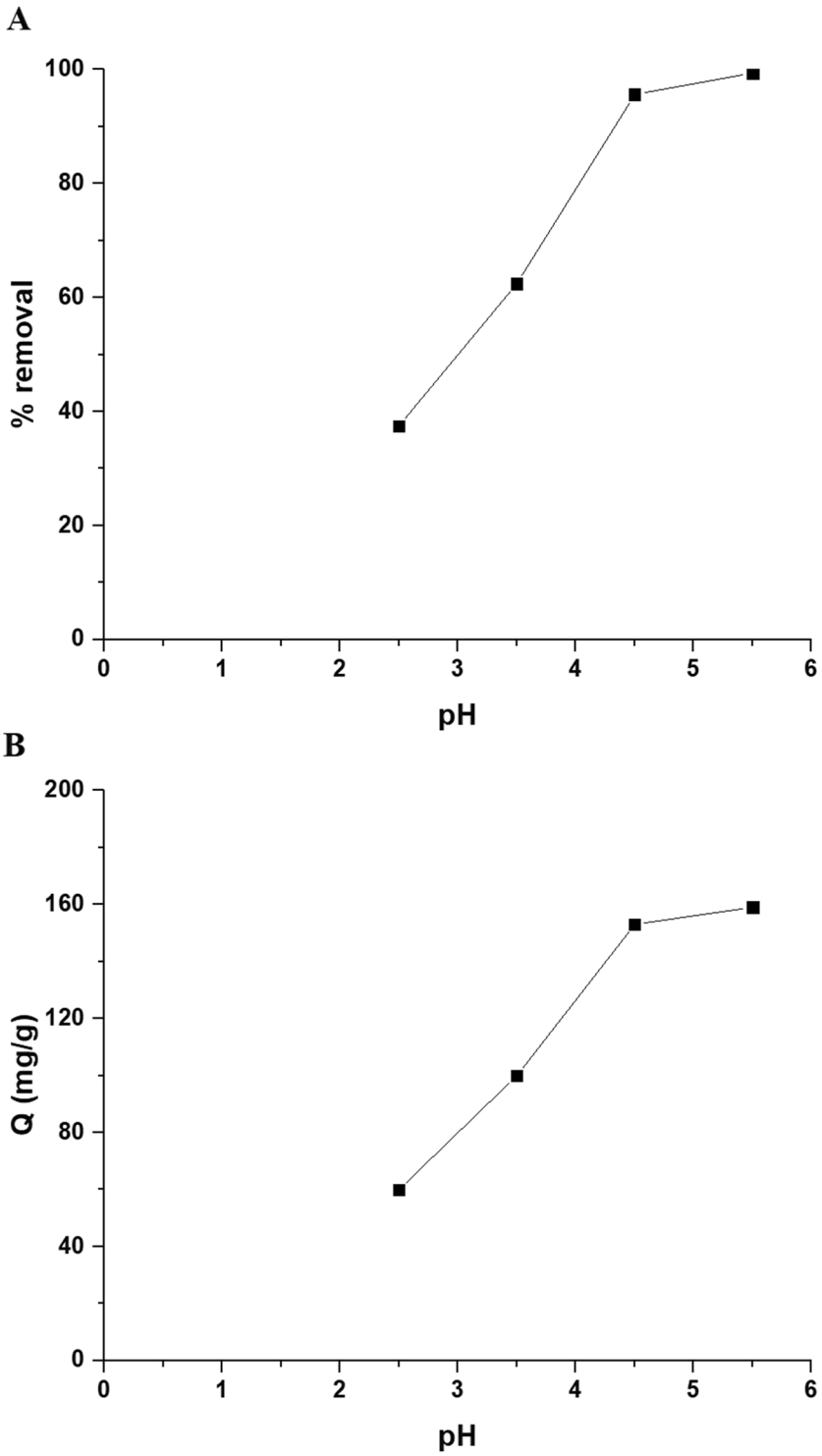

Fig. 6 The effect of solution pH on the % elimination of palladium (II) ions (**A**) and the elimination capability of the Co_2SiO_4/mordant red 3 nanocomposite (**B**). Experimental chemical conditions: Concentration = 160 mg/L; Volume = 60 mL; Amount of nanocomposite = 0.06 g; Time of adsorption = 120 min

cotton like structure in the Co_2SiO_4/mordant red 3 nanocomposite. Accordingly, this change in shape proves that the mordant red 3 was successfully loaded onto the Co_2SiO_4 nanoparticles [12, 19].

The obtained percentages of hydrogen (H), carbon (C), and nitrogen (N) in the Co_2SiO_4/mordant red 3 nanocomposite were estimated by the elemental analysis and found to be 3.32, 18.65, and 1.32%, respectively. Subsequently, the presence of nitrogen (N) and carbon (C) endorses the fruitful loading of the mordant red 3 on the Co_2SiO_4 nanoparticles, as shown in Scheme 1 [12, 19]. The energy dispersive X-ray spectroscopy (EDX) analysis of the Co_2SiO_4/mordant red 3 nanocomposite confirmed the presence of C, N, O, Co, Na, S, and Si as the basic components of the nanocomposite as shown in Fig. 5.

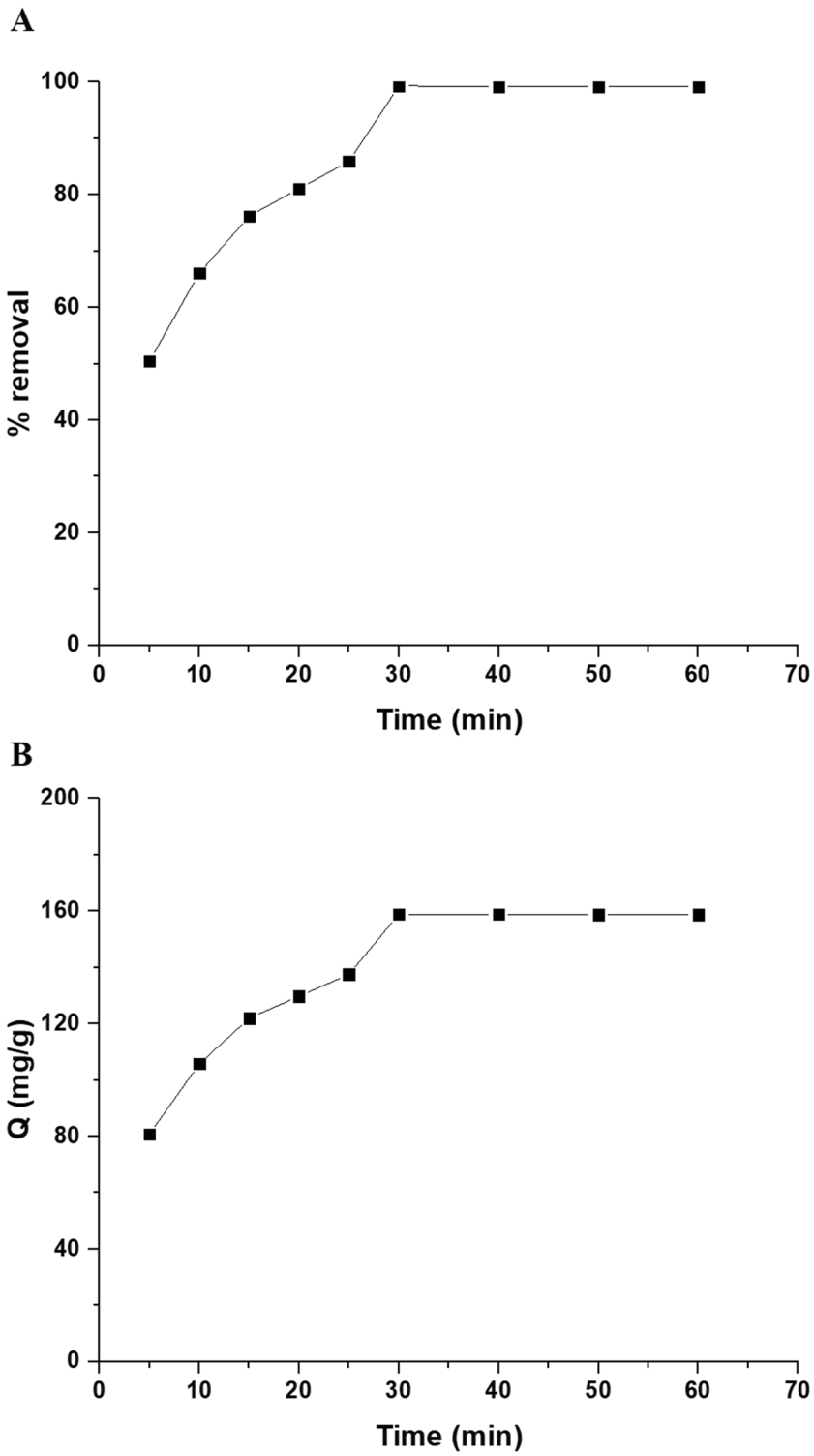

Fig. 7 The effect of time on the % removal of palladium (II) ions (**A**) and the elimination capability of the Co_2SiO_4/mordant red 3 nanocomposite (**B**). Experimental chemical conditions: Concentration = 160 mg/L; Volume = 60 mL; Amount of nanocomposite = 0.06 g; pH = 5.5

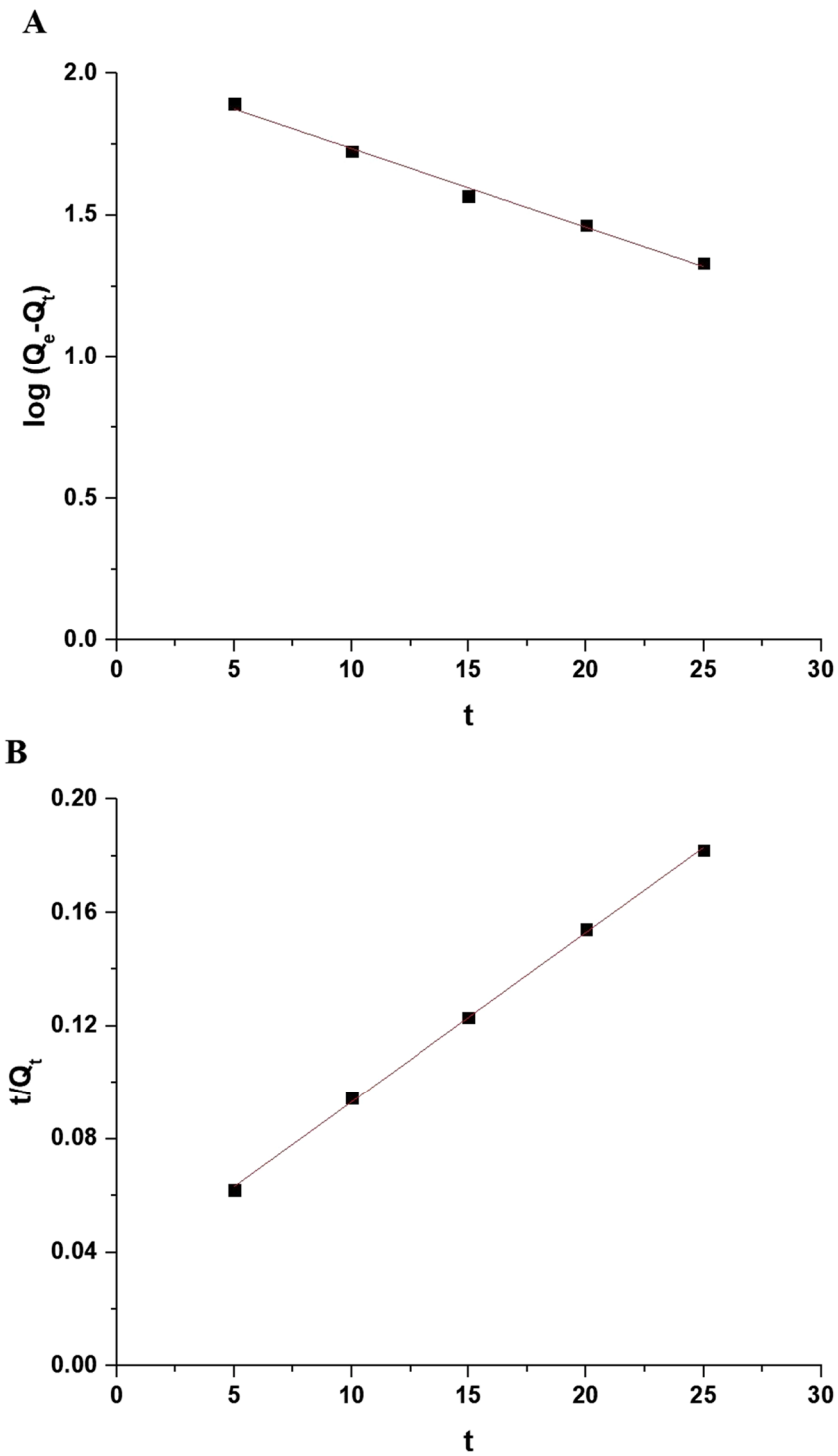

Fig. 8 Pseudo-1st -order (**A**) and pseudo-2nd -order (**B**) plots for the adsorption of palladium (II) ions onto the Co_2SiO_4/mordant red 3 nanocomposite

Table 1 The obtained constants of the pseudo-1st -order and pseudo-2nd -order kinetic equations for the adsorption of palladium (II) ions onto the Co_2SiO_4/mordant red 3 nanocomposite

Pseudo-first-order			Pseudo-first-order		
Q_e (mg/g)	K_1 (1/min)	R^2	Q_e (mg/g)	K_2 (g/mg.min)	R^2
102.82	0.0639	0.9897	166.94	0.00107	0.9991

Table 2 Thermodynamic parameters for the adsorption of palladium (II) ions onto the Co_2SiO_4/mordant red 3 nanocomposite

$\triangle H^o$ (KJ/mol)	$\triangle S^o$ (KJ/molK)	$\triangle G^o$ (KJ/mol)			
		298	308	318	328
-98.08	0.2906	-184.67	-187.57	-190.48	-193.39

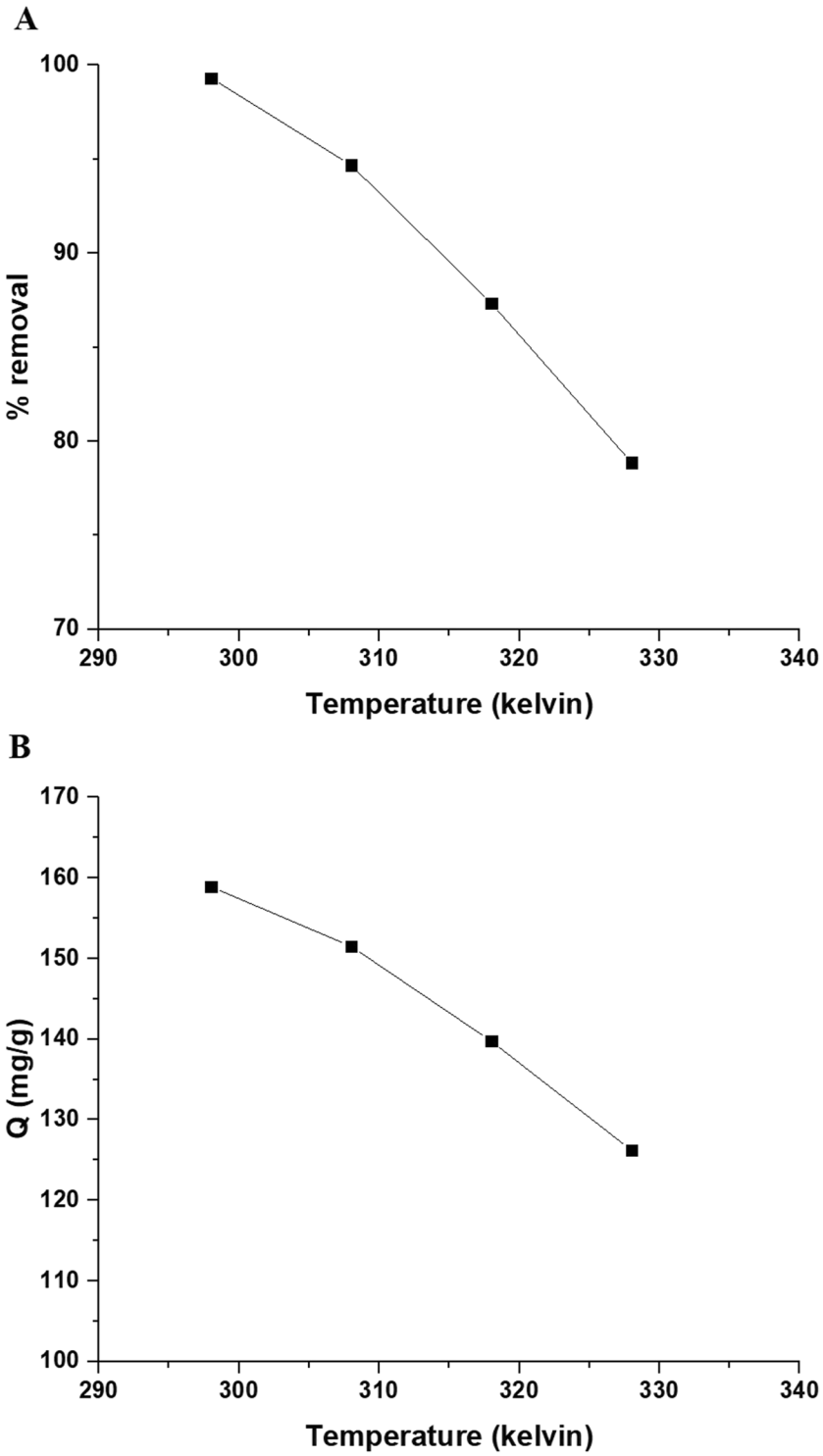

Fig. 9 The effect of solution temperature of solution on the % elimination of palladium (II) ions (**A**) and the elimination capability of the Co_2SiO_4/mordant red 3 nanocomposite (**B**). Experimental chemical conditions: Concentration = 160 mg/L; Volume = 60 mL; Amount of nanocomposite = 0.06 g; pH = 5.5; Time of adsorption = 30 min

3.2 Removal of Palladium (II) Ions from Aqueous Media

3.2.1 Effect of pH

pH is a critical aspect for the removal of metal ions using the solid phase extraction method because it directly impacts the behavior of functional groups found on the surface of the adsorbent, in addition to the species of ions present in the chemical solution. Besides, in order to verify the best pH of solution at which the maximum elimination of palladium ions occurred, the influence of solution pH from 2.5 to 5.5 was examined. Removal of palladium (II) ions at pH values greater than 5.5 has not been studied because of the

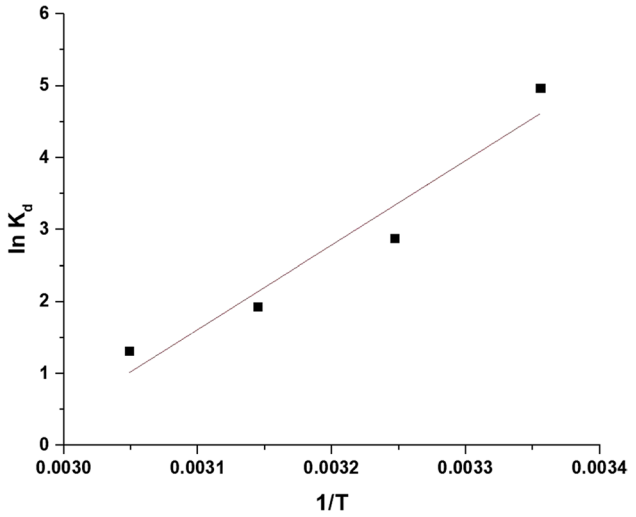

Fig. 10 The plot of ln K_d versus 1/T for the adsorption of palladium (II) ions onto the Co_2SiO_4/mordant red 3 nanocomposite

precipitation of palladium (II) ions as palladium hydroxide. Figure 6A-B exemplifies the effect of solution pH on the % removal of palladium (II) ions and the elimination capability of the Co_2SiO_4/mordant red 3 nanocomposite, respectively. The results demonstrate a considerable dependence between the elimination of palladium (II) ions onto the Co_2SiO_4/mordant red 3 nanocomposite and the initial pH of the palladium solution. Results demonstrated that the removal of palladium (II) ions increased as pH increased. This behavior may be a result of the competing adsorption of H^+ and palladium(II) ions onto the active groups of the Co_2SiO_4/mordant red 3 nanocomposite, which inhibits the removal of palladium (II) ions from strong acidic media [12, 19]. % Removal of palladium (II) ions and elimination capability of the Co_2SiO_4/mordant red 3 nanocomposite at pH = 5.5 are 99.38% and 159 mg/g, respectively. Consequently, for the next investigations, palladium (II) ions were removed simultaneously at pH = 5.5. In addition, the % elimination of palladium (II) ions and elimination capability of the Co_2SiO_4 at pH = 5.5 are 2.50% and 4 mg/g, respectively. Therefore, this confirms that the loaded material (i.e., mordant red 3) on the Co_2SiO_4 nanoparticles plays a very large role in removal of palladium (II) ions.

3.2.2 Effect of Time

Stirring time is a crucial aspect of the removal process because it indicates the rate of complete metal ion adsorption onto the surface of adsorbents. In order to determine the optimal time at which the maximum elimination of palladium (II) ions occurred, the influence of time from 5 to 60 min was examined. Figure 7A-B exemplifies the effect of elimination time on the % elimination of palladium (II) ions and the elimination capability of the Co_2SiO_4/mordant red 3 nanocomposite, respectively. The results demonstrate a considerable dependence between the elimination of palladium (II) ions onto the Co_2SiO_4/mordant red 3 nanocomposite and the stirring time. Results demonstrated that the removal of palladium (II) ions improved as elimination time improved from 5 to 30 min. After that, the rise in the removal of palladium (II) ion was insignificant as time increased from 30 to 60 min due to the saturation of active sites. % Removal of palladium (II) ions and elimination capability of the Co_2SiO_4/mordant red 3 nanocomposite at time = 30 min is 99.31% and 158.90 mg/g, respectively. Consequently, for the next investigations, palladium (II) ions were removed simultaneously at time = 30 min. The experimental results have been matched exploiting the pseudo-1st -order and pseudo-2nd -order kinetic equations as shown in Eqs. (4) and (5), respectively [12, 19].

$$\log\left(Q_e - Q_t\right) = logQ_e - \frac{K_1}{2.303}t \tag{4}$$

$$\frac{t}{Q_t} = \frac{1}{K_2 Q_e^2} + \frac{1}{Q_e}t \tag{5}$$

Q_t (mg/g) represents the amount of palladium (II) ions that adsorbed at elimination time t (min). Q_e (mg/g) represents the adsorption capability of the Co_2SiO_4/mordant red 3 nanocomposite at equilibrium, K_1 (1/min) exemplifies the rate constant for the pseudo-1st -order model, and K_2 (g/mg.min) exemplifies the rate constant for the pseudo-2nd -order model. In the case of the pseudo-first-order kinetic model, the equilibrium adsorption capacity (Q_e) and rate constant (K_1) for the removal of palladium (II) ions by Co_2SiO_4/mordant red 3 nanocomposite were obtained from the intercept and slope of the plot of log (Q_e-Q_t) versus time, as shown in Fig. 8A and Table 1. In the case of the pseudo-second-order kinetic model, the rate constant (K_2) and equilibrium adsorption capacity (Q_e) for the removal of palladium (II) ions by Co_2SiO_4/mordant red 3 nanocomposite were obtained from the intercept and slope of the plots of t/qt versus t, as shown in Fig. 8B and Table 1. The calculated correlation coefficient (R^2) for the pseudo-second order model is nearer to unity than that for the pseudo-first order model, showing that the elimination of palladium (II) ions using the Co_2SiO_4/mordant red 3 nanocomposite can be adequately described using the pseudo-second order model.

3.2.3 Effect of Temperature

Temperature is a crucial aspect of the removal process because it indicates the mechanism of adsorption. In order to determine the optimal temperature at which the maximum

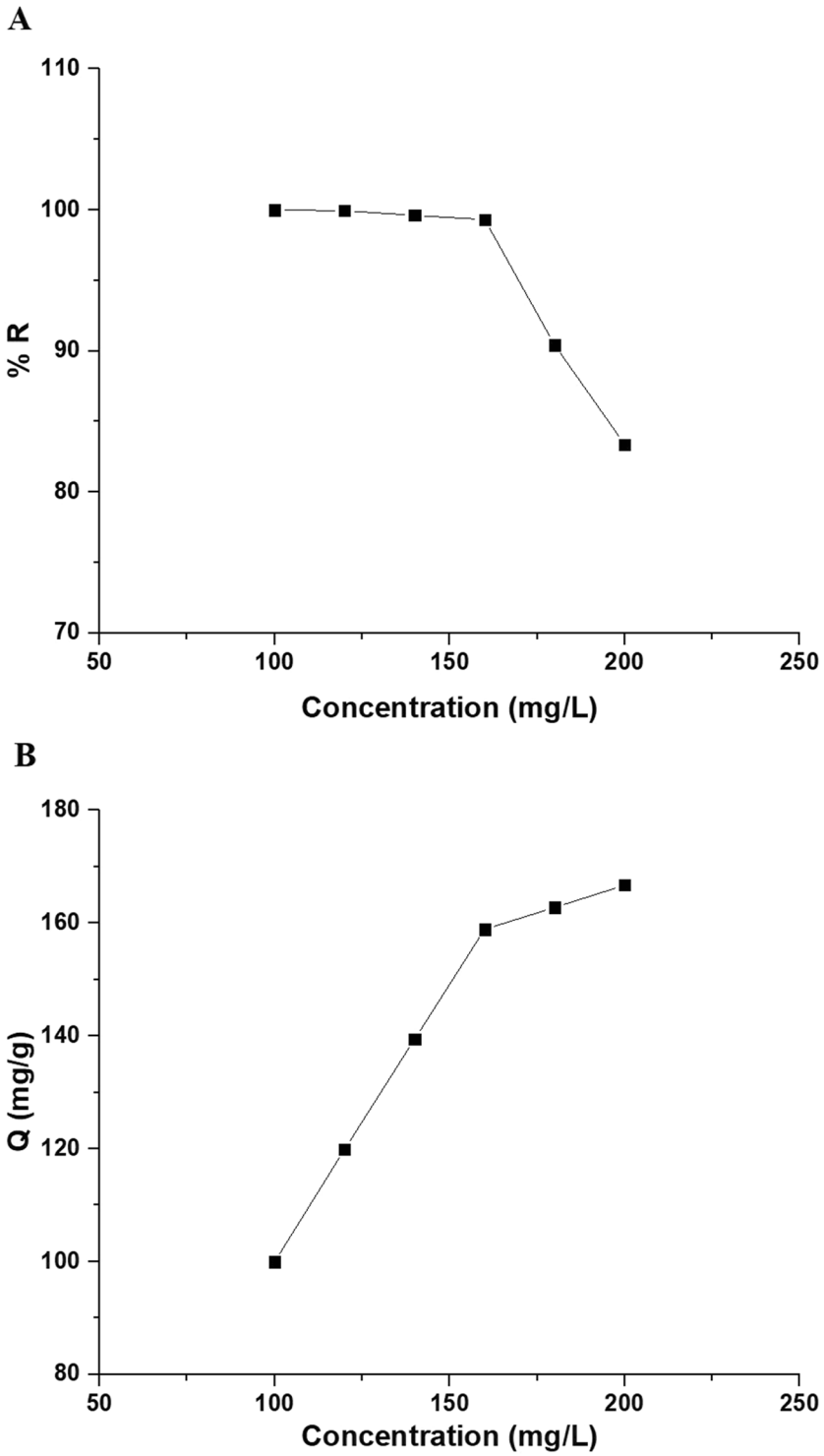

Fig. 11 The impact of concentration of palladium on the % elimination of palladium (II) ions (**A**) and the elimination capability of the Co_2SiO_4/mordant red 3 nanocomposite (**B**). Experimental chemical conditions: Volume = 60 mL; Amount of nanocomposite = 0.06 g; pH = 5.5; Time of adsorption = 30 min

elimination of palladium (II) ions occurred, the influence of temperature from 298 to 328 kelvin was examined. Figure 9A-B exemplifies the effect of temperature on the % elimination of palladium (II) ions and the elimination capability of the Co_2SiO_4/mordant red 3 nanocomposite, respectively. The results demonstrate a considerable dependence between the adsorption of palladium ions onto the Co_2SiO_4/

Table 3 The obtained constants of the applied Langmuir as well as Freundlich equilibrium isotherms for the adsorption of palladium (II) ions onto the Co_2SiO_4/mordant red 3 nanocomposite

Langmuir isotherm			Freundlich isotherm		
Q_W (mg/g)	K_L (L/mg)	R^2	Q_W (mg/g)	K_F (mg/g)(L/mg)$^{1/n}$	R^2
166.39	11.78	0.9998	193.09	140.88	0.8750

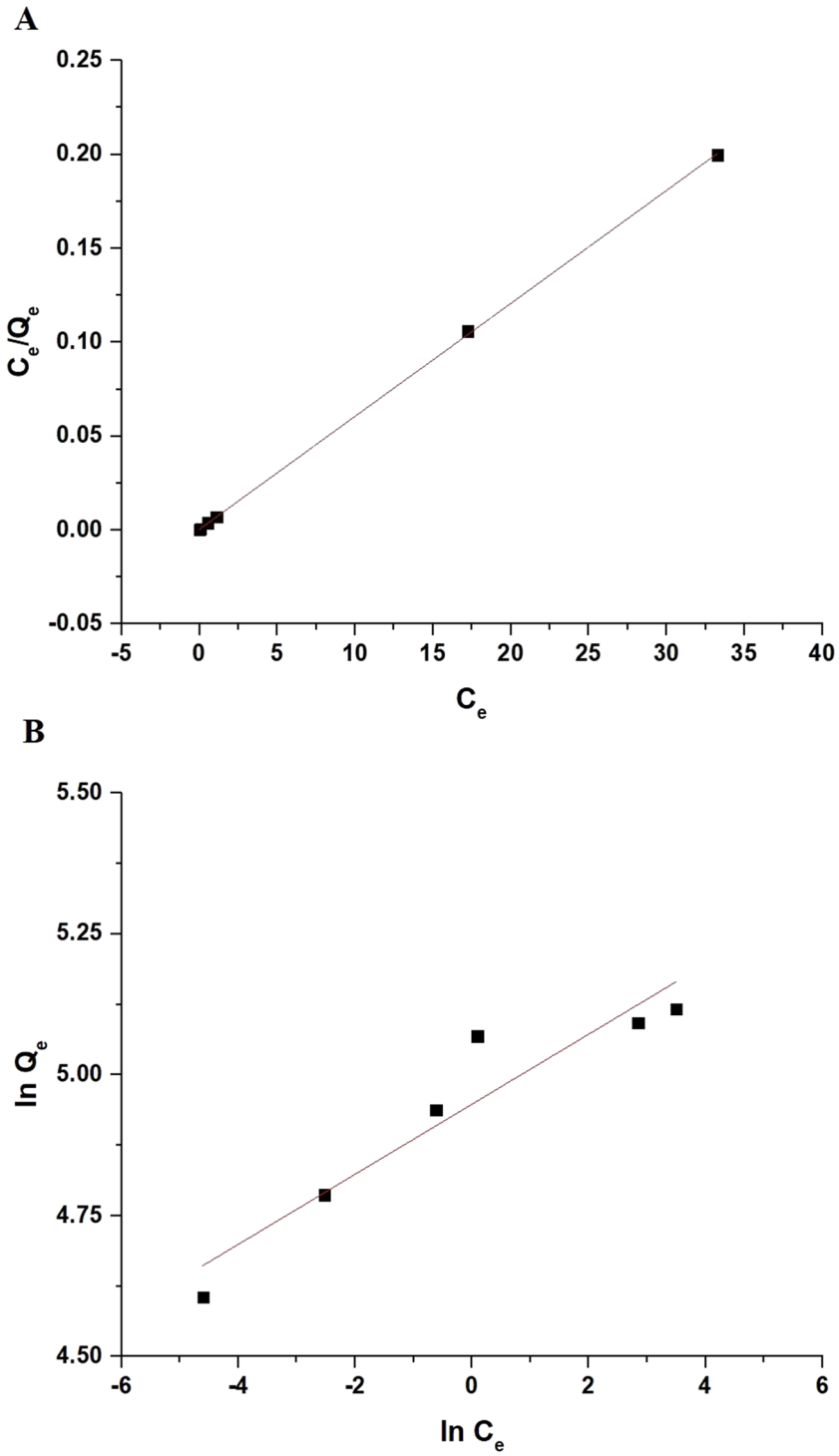

Fig. 12 Langmuir (**A**) and Freundlich (**B**) plots for the adsorption of palladium (II) ions onto the Co_2SiO_4/mordant red 3 nanocomposite

mordant red 3 nanocomposite and the temperature. The results demonstrated that the elimination of palladium (II) ions and elimination capability of the Co_2SiO_4/mordant red 3 nanocomposite decreased as solution temperature improved from 298 to 328 kelvin. The effect of solution temperature on the removal process of palladium (II) ions can be represented by calculating the thermodynamic factors, for example, change in free energy (ΔG^o, KJ/mol), change in entropy (ΔS^o, KJ/molK), and change in enthalpy (ΔH^o, KJ/mol) using Eqs. (6), (7), and (8) [12, 19].

Table 4 Comparison between the maximum elimination capability of the Co_2SiO_4/mordant red 3 nanocomposite and other adsorbents

Adsorbent	Q_W (mg/g)	Reference
MWCNTs modified by Poly (N-phenylethanolamine)	101	[32]
Alumina Nanopowder functionalized by Polyethyleneimine	97.7	[33]
Activated carbon functionalized by ethyl-3-(2-aminoethylamino)-2-chlorobut-2-enoate	92	[8]
MCM-41 modified with 3,4-dihydroxybenzaldehyde	155	[34]
Ferrofluid-based dispersive solid phase	24.6	[35]
Amberlite XAD-16 functionalized with 2-acetyl pyridine	8	[36]
Co_2SiO_4/mordant red 3 nanocomposite	166.39	This study

$$lnK_d = \frac{\triangle S^o}{R} - \frac{\triangle H^o}{RT} \quad (6)$$

$$\triangle G^o = \triangle H^o - T\triangle S^o \quad (7)$$

$$K_d = \frac{Q_e}{C_e} \quad (8)$$

where, T (kelvin) exemplifies the elimination solution temperature. In addition, K_d (L/g) exemplifies the constant of distribution process. Besides, R (kJ/mol kelvin) represents a gas constant. In addition, by drawing ln K_d versus 1/T, the values for ΔH^o and ΔS^o can be derived from the slope and intercept as shown in Fig. 10 and Table 2. In addition, ΔG^o values were determined depending on ΔS^o and ΔH^o values as shown in Table 2. The negative sign of ΔH^o indicates an exothermic process. Also, the value of ΔH^o is greater than about 40 KJ/mol, indicating a chemical elimination. The obtained positive value of (ΔS^o) indicates superior randomization at the solution/solid interface after elimination of the palladium (II) ions onto the Co_2SiO_4/mordant red 3 nanocomposite. The obtained negative values of ΔG^o indicated the spontaneous character of the elimination of palladium (II) ions employing the Co_2SiO_4/mordant red 3 nanocomposite.

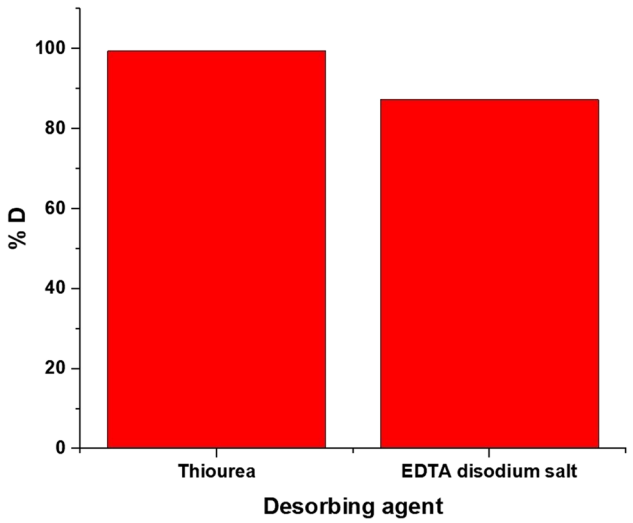

Fig. 13 Effect of different chemical eluents on the desorption of palladium (II) ions from the Co_2SiO_4/mordant red 3 nanocomposite. Experimental chemical conditions: Concentration of palladium solution = 5 mg/L; Concentration of eluent solution = 0.5 mol/L; Volume of palladium solution = 60 mL; Volume of eluent solution = 6 mL; Amount of nanocomposite = 0.06 g; pH = 5.5; Time of adsorption = 30 min

3.2.4 Effect of Palladium Concentration

The initial solution concentration of the metal ions is a vital aspect of the removal process because it indicates the maximum adsorption capacity of the adsorbent. In order to determine the maximum adsorption capacity of palladium (II) ions, the influence of concentration from 100 to 200 mg/L was examined. Figure 11A-B exemplifies the influence of concentration of palladium on the % elimination of palladium (II) ions and the elimination capability of the Co_2SiO_4/mordant

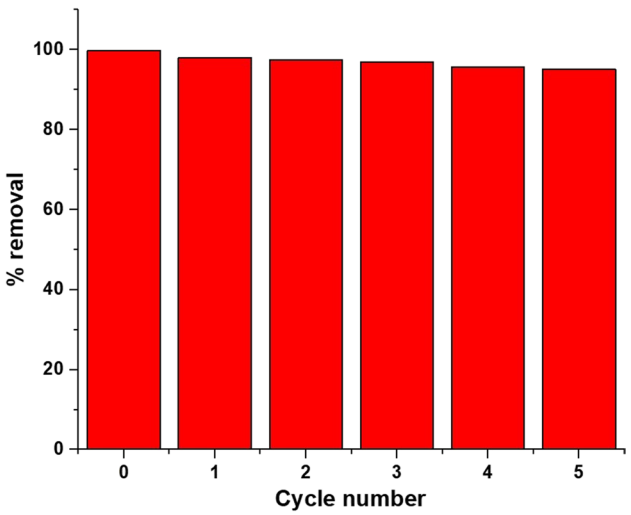

Fig. 14 Reusability of the Co_2SiO_4/mordant red 3 nanocomposite in the adsorption of palladium (II) ions

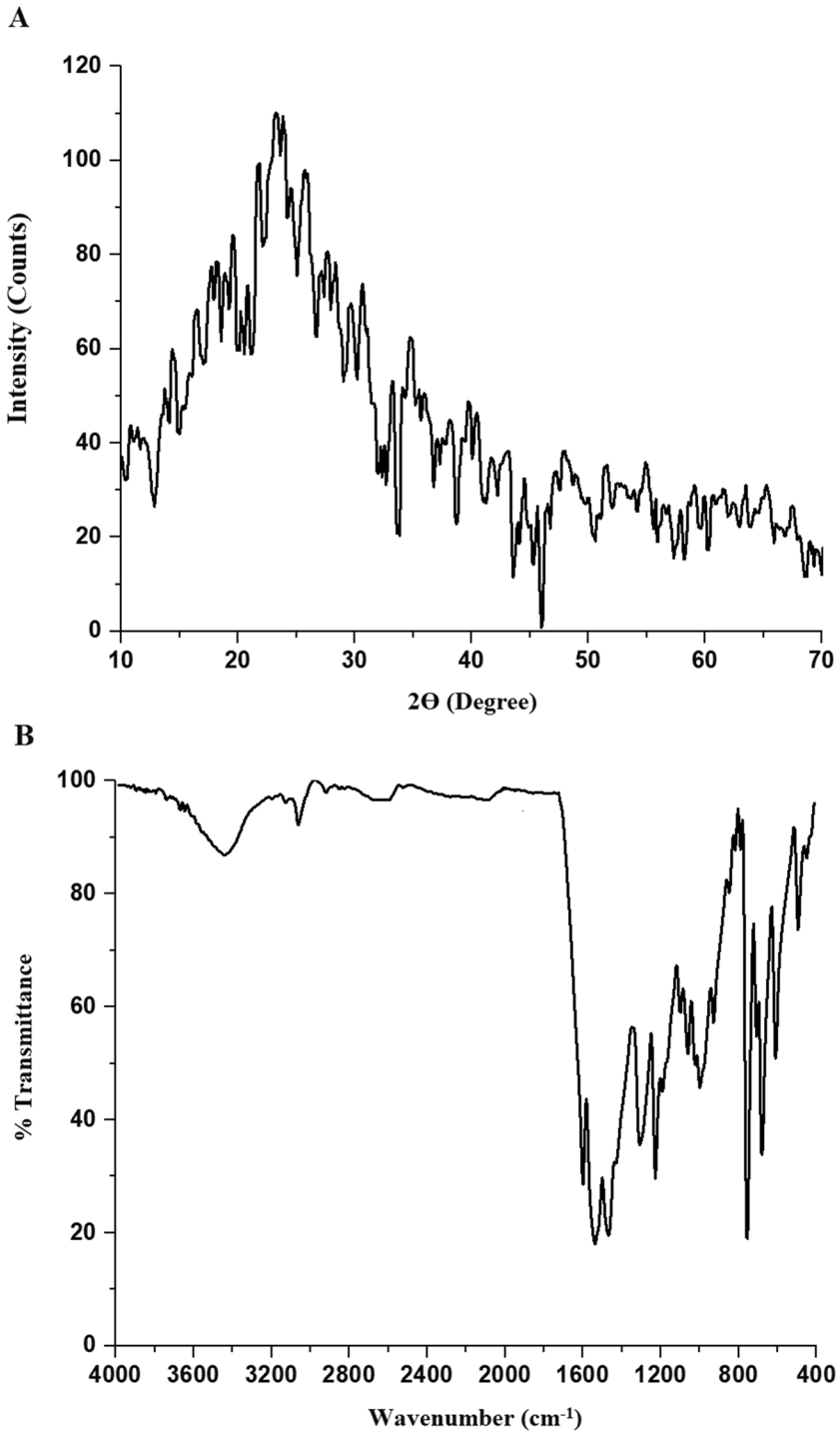

Fig. 15 XRD (**A**) and FT-IR (**B**) of the regenerated nanocomposite

red 3 nanocomposite, respectively. The results demonstrate a considerable dependence between the adsorption of palladium (II) ions onto the Co_2SiO_4/mordant red 3 nanocomposite and the concentration. Results demonstrated that the removal of palladium (II) ions decreased whereas adsorption capacity increased as concentration increased from 100 to 200 mg/L. The experimental results have been matched exploiting the Langmuir as well as Freundlich equilibrium isotherms as shown in Eqs. (9) and (10), respectively [12, 19].

$$\frac{C_e}{Q_e} = \frac{1}{K_L Q_W} + \frac{C_e}{Q_W} \tag{9}$$

$$lnQ_e = lnK_F + \frac{1}{n} lnC_e \tag{10}$$

where, K_L (L/mg) and Q_W (mg/g) are the equilibrium constant and maximum elimination capability of the applied Langmuir equilibrium isotherm, respectively. Also, K_F

Table 5 Tolerance limits of several interfering ions in the determination of 100 µg/L of palladium (II) solution

Interfering ion	Tolerance limit (µg/L)	% R
Na(I)	3500	99.58
K(I)	3500	98.67
Mg(II)	3500	97.52
Ni(II)	3000	96.78
Cd(II)	1000	96.93
Co(II)	1000	97.29
Pb(II)	450	96.85
Ba(II)	450	97.32
Cu(II)	200	96.29
Fe(III)	200	96.75
Cr(III)	800	96.78
SO_4^{-2}	3500	98.89
HCO_3^-	1000	98.48
Br^-	1000	97.83
SCN^-	1000	99.26

(mg/g) $(L/mg)^{1/n}$ and 1/n exemplifies the equilibrium constant and the heterogeneity constant of the applied Freundlich equilibrium isotherm, respectively. In addition, the Langmuir isotherm is the most straightforward theoretical isotherm for monolayer adsorption onto a surface with a specific number of identical sites. By plotting C_e/Q_e versus C_e, it is possible to determine the Q_m and K_L, as shown in Fig. 12A and Table 3. The Freundlich isotherm is an empirical equation appropriate for both multilayer and non-ideal adsorption on heterogeneous surfaces. By plotting ln Q_e versus ln C_e, it is possible to determine the K_F and 1/n, as shown in Fig. 12B and Table 3. The applied Freundlich isotherm can be exploited to estimate the maximum elimination capability (Q_W) by Eq. (11) [12, 19].

$$Q_W = K_F\left(C_o^{1/n}\right) \tag{11}$$

The calculated correlation coefficient (R^2) for the Langmuir isotherm is greater than that for the Freundlich isotherm, showing that the adsorption of palladium (II) ions using the Co_2SiO_4/mordant red 3 nanocomposite can be adequately described using the Langmuir isotherm. The maximum adsorption capacity of the Co_2SiO_4/mordant red 3 nanocomposite towards palladium (II) ions is 166.39 mg/g, which is greater than that of other adsorbents in the literature as shown in Table 4 [8, 32–36].

3.2.5 Impact of Desorption and Reusability

For the desorption of palladium (II) ions from the Co_2SiO_4/mordant red 3 nanocomposite, various eluents (thiourea as well as ethylenediaminetetraacetic acid disodium salt dihydrate) were examined. Figure 13 demonstrates that thiourea at a concentration of 0.5 mol/L had the greatest ability (% D = 99.49%) to desorb palladium (II) ions from the Co_2SiO_4/mordant red 3 nanocomposite. To determine the reusability of the Co_2SiO_4/mordant red 3 nanocomposite, five sequential adsorption and desorption cycles were performed. The data depicted in Fig. 14 demonstrate that the % removal value is nearly constant after five cycles. Consequently, the Co_2SiO_4/mordant red 3 nanocomposite maintained its removal effectiveness.

Both the XRD and FT-IR analyses of the regenerated nanocomposite proved that there is no difference in the locations or intensity of the nanocomposite, which confirms its stability as shown in Fig. 15A-B, respectively.

3.2.6 Impact of Interference

To determine the impact of assorted interfering ions (cations and anions) on the elimination efficacy of palladium (II) ions exploiting the Co_2SiO_4/mordant red 3 nanocomposite, several concentrations of the interfering ions were mixed individually with a 60 mL of 100 µg/L of palladium (II) solution. The elimination technique was carried out exactly as depicted earlier, and its usefulness was assessed. The tolerance limit was recognized as the highest concentration of the interfering ion that resulted in a 5% extraction error. The data shown in Table 5 indicate that the studied interfering ions did not affect the extraction of palladium (II) ions. Accordingly, the elimination method can be directed to the analysis of palladium (II) ions in real samples, including various components.

Table 6 Estimation of palladium (II) ions in spiked samples after separation and preconcentration using the Co_2SiO_4/mordant red 3 nanocomposite

Sample	Found concentration	Added volume (0.2 mL)			Added volume (0.40 mL)		
		Found concentration (µg/L)	% Recovery	% RSD	Found concentration (µg/L)	% Recovery	% RSD
Seawater	BDL	3.28 ± 0.0555	98.73	1.55	6.50 ± 0.1520	98.15	1.88
River water	BDL	3.30 ± 0.0760	99.33	1.86	6.56 ± 0.1883	99.06	2.31

BDL means below detection limit

3.2.7 Application

Seawater and river water samples were collected in polypropylene containers from a depth of one meter below the surface of the water. After that, they were filtered to get rid of suspended solids and stored at -22°C. The propositioned elimination method was devoted to preconcentrate palladium (II) ions in some real environmental samples (river water and Sea water) prior to the atomic absorption spectrometer analysis as previously described. Also, different volumes (0.2 and 0.4 mL) of palladium (II) ions with a concentration of 1000 µg/L were added to 60 mL of water sample then the preconcentration method was employed as previously described. The results confirmed that the optimized procedure has a 0.5 to 450 µg/L dynamic linear range. Also, the limit of detection (LOD), which was determined using Eq. (12), equals 0.14 µg/L [12, 13].

$$LOD = 3\frac{SD}{S} \tag{12}$$

where, S and SD are the slope of calibration curve and standard deviation, respectively. Besides, % recovery and % RSD were determined using Eqs. (13) and (14), respectively.

$$\%\ Recovery = \frac{Found\ practical\ concentration}{Theoretical\ concentration} \times 100 \tag{13}$$

$$\%RSD = \frac{SD}{Mean} \times 100 \tag{14}$$

Furthermore, found palladium concentrations were symbolized as (average ± (SD×t/$\sqrt{u}$). where, u (no of chemical determinations) = 5. In addition, critical value (t) = 2.78, and level of confidence = 95%. Table 6 displays the results of the preconcentration of palladium (II) ions along with the recoveries for the spiked samples. The values of % recovery was greater than 95% and hence this indicates that the elimination process is adaptable, accurate, and resulted in chemical quantitative elimination. Additionally, the obtained % RSD was less than 3.5% and hence this indicates good reproducibility.

4 Conclusions

Using the Pechini sol gel process, Co_2SiO_4 nanoparticles were produced and then modified with mordant red 3 as a new nanocomposite for the separation and analytical preconcentration of palladium (II) ions from the aqueous chemical solutions prior to their measurement by atomic absorption spectroscopy. The maximum adsorption capability of the synthesized nanocomposite towards palladium (II) ions is 166.39 mg/g. The results confirmed that the optimized procedure is accurate (% recovery > 95%), reproducible (% RSD < 3.5%), and has a 0.5 to 450 µg/L dynamic linear range.

Author Contributions Faisal K Algethami conducted experimental work, organized the experimental results, wrote the manuscript, and corresponded the manuscript for publication.

Data Availability Data will be made available on request.

Declarations

Ethics Approval Author approves that the submitted work is original and has not been published elsewhere in any form or language (partially or in full).

Consent to Participate Yes.

Consent for Publication Yes.

Conflict of Interest The author declares that he has no conflict ofinterest.

References

1. Ye FY, Hu M, Yu W, Zheng YS (2022) Highly selective detection of palladium ions by sulfur-containing tetraphenylethylene tetracycle helicate. Dye Pigment 208:110857. https://doi.org/10.1016/j.dyepig.2022.110857
2. Aruguete DM, Wallace A, Blakney T et al (2020) Palladium release from catalytic converter materials induced by road de-icer components chloride and ferrocyanide. Chemosphere 245:125578. https://doi.org/10.1016/j.chemosphere.2019.125578
3. Kielhorn J, Melber C, Keller D, Mangelsdorf I (2002) Palladium - A review of exposure and effects to human health. Int J Hyg Environ Health 205:417–432. https://doi.org/10.1078/1438-4639-00180
4. Zhang N, Ma Y, Shen Y, Gao X (2014) Determination of platinum, palladium, ruthenium, rhodium, and iridium in ultrabasic rock from the Great Dyke of Zimbabwe by inductively coupled plasma-optical emission spectrometry. Anal Lett 47:2072–2079. https://doi.org/10.1080/00032719.2014.893441
5. Müller M, Heumann KG (2000) Isotope dilution inductively coupled plasma quadrupole mass spectrometry in connection with a chromatographic separation for ultra trace determinations of platinum group elements (pt, pd, Ru, ir) in environmental samples. Fresenius J Anal Chem 368:109–115. https://doi.org/10.1007/s002160000494
6. Tokalioğlu Ş, Oymak T, Kartal Ş (2004) Determination of palladium in various samples by atomic absorption spectrometry after preconcentration with dimethylglyoxime on silica gel. Anal Chim Acta 511:255–260. https://doi.org/10.1016/j.aca.2004.02.015
7. Mori I, Kawakatsu T, Fujita Y, Matsuo T (1999) Selective spectrophotometric determination of palladium(II) with 2(5- nitro-2-pyridylazo)-5-(N-propyl-N-3-sulfopropylamino)phenol(5-NO2. PAPS) and tartaric acid with 5-NO2.PAPS-niobium(V) complex. Talanta 48:1039–1044. https://doi.org/10.1016/S0039-9140(98)00309-9
8. Tu Z, Lu S, Chang X et al (2011) Selective solid-phase extraction and separation of trace gold, palladium and platinum using activated carbon modified with ethyl-3-(2-aminoethylamino)-2-chlorobut-2-enoate. Microchim Acta 173:231–239. https://doi.org/10.1007/s00604-011-0552-0
9. Mohammadi SZ, Afzali D, Taher MA, Baghelani YM (2010) Determination of trace amounts of palladium by flame atomic absorption spectrometry after ligandless-dispersive liquid-liquid

microextraction. Microchim Acta 168:123–128. https://doi.org/10.1007/s00604-009-0267-7
10. Hassanien MM, Mortada WI, Kenawy IM (2015) Selective separation of palladium from synthetic highly active liquid waste by cloud point extraction using benzil mono-(2-pyridyl)hydrazone and Triton X-114. J Radioanal Nucl Chem 303:261–269. https://doi.org/10.1007/s10967-014-3430-5
11. Hu Q, Yang X, Huang Z et al (2005) Simultaneous determination of palladium, platinum, rhodium and gold by on-line solid phase extraction and high performance liquid chromatography with 5-(2-hydroxy-5-nitrophenylazo)thiorhodanine as pre-column derivatization regents. J Chromatogr A 1094:77–82. https://doi.org/10.1016/j.chroma.2005.07.090
12. Al-Wasidi AS, Naglah AM, Saad FA, Abdelrahman EA (2022) Modification of sodium aluminum silicate hydrate by thioglycolic acid as a new composite capable of removing and preconcentrating pb(II), Cu(II), and zn(II) ions from food and water samples. Arab J Chem 15:104178. https://doi.org/10.1016/j.arabjc.2022.104178
13. Al-Wasidi AS, AlSalem HS, Alshalawi AF et al (2022) Facile synthesis of a novel nanocomposite for determination of mercury and copper ions in food and water samples. Arab J Chem 15:104113. https://doi.org/10.1016/j.arabjc.2022.104113
14. Parastar M, Sheshmani S, Shokrollahzadeh S (2021) Cross-linked chitosan into graphene oxide-iron(III) oxide hydroxide as nano-biosorbent for pd(II) and cd(II) removal. Elsevier B.V, Amsterdam
15. Monier M, Abdel-Latif DA, Abou El-Reash YG (2016) Ion-imprinted modified chitosan resin for selective removal of pd(II) ions. J Colloid Interface Sci 469:344–354. https://doi.org/10.1016/j.jcis.2016.01.074
16. Kumar R, Sharma RK, Singh AP (2019) Grafting of cellulose with N-isopropylacrylamide and glycidyl methacrylate for efficient removal of Ni(II), Cu(II) and pd(II) ions from aqueous solution. Sep Purif Technol 219:249–259. https://doi.org/10.1016/j.seppur.2019.03.035
17. Naini N, Sid Kalal H, Almasian MR et al (2022) Phosphine-functionalized Fe3O4/SiO2/composites as efficient magnetic nanoadsorbents for the removal of palladium ions from aqueous solution: kinetic, thermodynamic and isotherm studies. Mater Chem Phys 287:126242. https://doi.org/10.1016/j.matchemphys.2022.126242
18. Gad HM, El Rayes SM, Abdelrahman EA (2022) Modification of silica nanoparticles by 2,4-dihydroxybenzaldehyde and 5-bromosalicylaldehyde as new nanocomposites for efficient removal and preconcentration of Cu(ii) and cd(ii) ions from water, blood, and fish muscles. RSC Adv 12:19209–19224. https://doi.org/10.1039/d2ra03177a
19. Khalifa ME, Abdelrahman EA, Hassanien MM, Ibrahim WA (2020) Application of mesoporous silica nanoparticles modified with dibenzoylmethane as a novel composite for efficient removal of cd(II), hg(II), and Cu(II) ions from aqueous media. J Inorg Organomet Polym Mater 30:2182–2196. https://doi.org/10.1007/s10904-019-01384-w
20. Bayat S, Sobhani A, Salavati-Niasari M (2018) Co2SiO4 nanostructures/nanocomposites: synthesis and investigations of optical, magnetic, photocatalytic, thermal stability and flame retardant properties. J Mater Sci Mater Electron 29:7077–7089. https://doi.org/10.1007/s10854-018-8695-y
21. Guo P, Wang C (2015) Synthesis and lithium storage performance of Co2SiO4 nanoparticles. RSC Adv 5:70661–70667. https://doi.org/10.1039/c5ra11327j
22. Vaselnia SY, Khajeh Aminian M, Dehghan Banadaki R (2022) Experimental and theoretical study on the structural, electronic, and optical properties within DFT + U, Fxc kernel for LRC model, and BSE approaches. Part II: CoSiO3 and Co2SiO4 pigments. Powder Technol 397:116999. https://doi.org/10.1016/j.powtec.2021.11.043
23. Mu Y, Zhang Y, Pei X et al (2022) Dispersed FeOx nanoparticles decorated with Co2SiO4 hollow spheres for enhanced oxygen evolution reaction. J Colloid Interface Sci 611:235–245. https://doi.org/10.1016/j.jcis.2021.12.099
24. Stoia M, Stefanescu M, Dippong T et al (2010) Low temperature synthesis of Co2SiO4/SiO2 nanocomposite using a modified sol-gel method. J Sol-Gel Sci Technol 54:49–56. https://doi.org/10.1007/s10971-010-2156-2
25. Shojaei B, Miri R, Bazyari A, Thompson LT (2022) Asphaltene adsorption on MgO, CaO, SiO2, and Al2O3 nanoparticles synthesized via the Pechini-type Sol – Gel method. Fuel 321:124136. https://doi.org/10.1016/j.fuel.2022.124136
26. Mirzaei A, Janghorban K, Hashemi B et al (2016) Highly stable and selective ethanol sensor based on α-Fe2O3 nanoparticles prepared by Pechini sol-gel method. Ceram Int 42:6136–6144. https://doi.org/10.1016/j.ceramint.2015.12.176
27. Chrunik M, Majchrowski A, Zasada D et al (2017) Modified Pechini synthesis of Bi2ZnB2O7 nanoparticles. J Alloys Compd 725:587–597. https://doi.org/10.1016/j.jallcom.2017.07.172
28. Zinatloo-Ajabshir S, Salavati-Niasari M (2019) Preparation of magnetically retrievable CoFe2O4@SiO2@Dy2Ce2O7 nanocomposites as novel photocatalyst for highly efficient degradation of organic contaminants. Compos Part B Eng 174:106930. https://doi.org/10.1016/j.compositesb.2019.106930
29. Boullosa-Eiras S, Vanhaecke E, Zhao T et al (2011) Raman spectroscopy and X-ray diffraction study of the phase transformation of ZrO2-Al2O3 and CeO2-Al 2O3 nanocomposites. Catal Today 166:10–17. https://doi.org/10.1016/j.cattod.2010.05.038
30. Youssef HM, Shah RK, Algethami FK et al (2021) Facile hydrothermal procedure for the synthesis of sodium aluminum silicate hydrate/analcime and analcime for effective removal of manganese(II) ions from aqueous solutions. J Inorg Organomet Polym Mater 31:1035–1046. https://doi.org/10.1007/s10904-020-01699-z
31. Almutairi MA, Algethami FK, Youssef HM (2020) Facile fabrication of novel analcime / sodium aluminum silicate hydrate and zeolite Y / faujasite mesoporous nanocomposites for efficient removal of Cu (II) and pb (II) ions from aqueous media. Integr Med Res 9:7900–7914. https://doi.org/10.1016/j.jmrt.2020.05.052
32. Behbahani M, Bagheri A, Gorji T et al (2013) Application of poly (N-phenylethanolamine) modified MWCNTs as a new sorbent for solid-phase extraction of trace palladium ions in soil and water samples. Sample Prep 1:10–17. https://doi.org/10.2478/sampre-2013-0002
33. Nagarjuna R, Sharma S, Rajesh N, Ganesan R (2017) Effective adsorption of precious metal palladium over polyethyleneimine-functionalized alumina nanopowder and its reusability as a catalyst for energy and environmental applications. ACS Omega 2:4494–4504. https://doi.org/10.1021/acsomega.7b00431
34. Behbahani M, Najafi F, Amini MM et al (2014) Solid phase extraction using nanoporous MCM-41 modified with 3,4-dihydroxybenzaldehyde for simultaneous preconcentration and removal of gold(III), palladium(II), copper(II) and silver(I). J Ind Eng Chem 20:2248–2255. https://doi.org/10.1016/j.jiec.2013.09.057
35. Farahani MD, Shemirani F, Gharehbaghi M (2013) Ferrofluid-based dispersive solid phase extraction of palladium. Talanta 109:121–127. https://doi.org/10.1016/j.talanta.2013.01.061
36. Ruhela R, Singh KK, Tomar BS et al (2012) Amberlite XAD-16 functionalized with 2-acetyl pyridine group for the solid phase extraction and recovery of palladium from high level waste solution. Sep Purif Technol 99:36–43. https://doi.org/10.1016/j.seppur.2012.08.018